antioxidants

MDPI

Article

Eriodictyol Modulates Cell-Type-Specific Stress Response Pathways In Vitro and Improves Visible Signs of Skin Aging

Taylor Oswald, Zixuan Shao, Daniel Zambrano, Jillian M. Freese, Elizabeth B. Ludes and Nicholas J. Brideau *

Debut Biotechnology, Inc., 11545 Sorrento Valley Road, Suite 310, San Diego, CA 92121, USA; toswald@debutbiotech.com (T.O.); zshao@debutbiotech.com (Z.S.); dzambrano@debutbiotech.com (D.Z.); lbentley@debutbiotech.com (E.B.L.)
* Correspondence: nbrideau@debutbiotech.com; Tel.: +1-800-982-3029 (ext. 703)

Abstract

Skin aging involves progressive disruption of redox balance, proteostasis, inflammation, and extracellular matrix integrity. Flavonoids have attracted interest for their ability to regulate cellular stress responses relevant to these processes. This study investigated the natural flavonoid eriodictyol (EDL) in human skin cells and evaluated whether topical application improved visible skin quality. Primary human keratinocytes and dermal fibroblasts were treated with EDL and profiled by RNA-sequencing to characterize cell-type-specific transcriptional responses. Functional validation assessed oxidative stress, inflammatory signaling, and senescence-associated markers, while a seven-flavonoid structure-function comparison contextualized EDL activity. Topical effects were assessed in a randomized, double-blind, vehicle-controlled cosmetic study ($N = 60$) using an EDL-containing formulation for 12 weeks. EDL induced distinct transcriptional changes in keratinocytes and fibroblasts, with enrichment of unfolded protein response pathways in both cell types. Keratinocytes showed increased expression of antioxidant and autophagy-related genes, whereas fibroblasts showed changes in gene expression pathways related to proliferation, metabolism, and senescence signaling. Functional assays further showed that EDL reduced intracellular reactive oxygen species, inflammatory cytokine secretion, and senescence-associated β-galactosidase activity. In a 12-week topical evaluation, EDL significantly improved overall skin quality across multiple parameters of visible aging compared with the vehicle. These findings demonstrate that EDL modulates stress-response pathways in human skin cells and improves visible skin quality following topical application.

Keywords: eriodictyol; NRF2 signaling; senescence; oxidative stress; autophagy; keratinocytes; dermal fibroblasts; skin aging; flavonoids

Check for updates

Academic Editor: Maria Letizia Manca

Received: 14 May 2026
Revised: 3 November 2026
Accepted: 5 November 2026
Published: 7 November 2026

Copyright: © 2026 by the authors. Licensee MDPI, Basel, Switzerland. This article is an open access article distributed under the terms and conditions of the Creative Commons Attribution (CC BY) license.

1. Introduction

Skin aging is characterized by progressive changes in redox and protein homeostasis, extracellular matrix (ECM) organization, and communication between epidermal and dermal compartments. Chronic exposure to ultraviolet radiation, pollution, and other environmental stressors increases reactive oxygen species (ROS) production and inflammatory signaling, contributing to cumulative cellular dysfunction. In keratinocytes, oxidative stress affects differentiation programs, lipid organization, barrier maintenance, and inflammatory signaling through multiple pathways including NF-κB [1,2]. In the dermis, increased matrix metalloproteinase (MMP) activity and reduced fibroblast biosynthetic capacity contribute

to collagen fragmentation, ECM disorganization, and impaired tissue remodeling [3]. These processes are further influenced by the accumulation of senescent cells, which release inflammatory cytokines, proteases, and matrix-remodeling factors collectively termed the senescence-associated secretory phenotype (SASP) [4,5]. Together, these interconnected processes contribute to progressive changes in skin structure and function during aging.

Maintenance of skin homeostasis depends on adaptive pathways that regulate oxidative stress, inflammation, and proteostasis. Oxidative stress, for instance, is regulated by nuclear factor erythroid 2-related factor 2 (NRF2). NRF2 is a central regulator of cellular antioxidant defense, controlling expression of enzymes involved in redox regulation, glutathione metabolism, and protection against oxidative stress [6]. In skin, NRF2 signaling contributes to keratinocyte differentiation, epidermal barrier maintenance, and regulation of inflammatory responses [7]. Proteostasis, on the other hand, is maintained by the unfolded protein response (UPR). UPR maintains protein homeostasis during endoplasmic reticulum (ER) stress by regulating protein folding, translation, and degradation pathways [8]. These two pathways (NRF2 and UPR) are interconnected through multiple mechanisms, such as PERK-dependent activation of the integrated stress response, providing a link between redox regulation and proteostasis [9,10]. Disruption of these adaptive pathways has been associated with inflammation, cellular senescence, and ECM deterioration during skin aging. Compounds capable of modulating these stress-response pathways across multiple skin cell types may therefore provide opportunities to influence age-associated changes in skin biology.

Flavonoids are a diverse class of plant-derived compounds that regulate oxidative stress, inflammatory signaling, and cellular stress responses across biological systems [11,12]. Several polyphenols and flavonoids have been characterized as potential hormetic compounds that can activate endogenous stress-response pathways in skin cells, influencing cellular resilience and tissue-associated functions [13]. Consistent with these findings, topical compounds that influence cellular stress pathways have demonstrated improvements in selected measures of facial skin appearance [14].

Eriodictyol (EDL), a flavanone found in citrus species and aromatic herbs, has been investigated for its antioxidant and anti-inflammatory properties. EDL exhibits diverse biological activities in preclinical models, including neuroprotective, cardioprotective, hepatoprotective, metabolic, and anticancer effects through regulation of multiple signaling pathways [15–17]. In skin-relevant models, EDL has demonstrated protective effects against UV-induced damage in keratinocytes, including antioxidant and anti-apoptotic activity associated with modulation of stress-responsive signaling pathways [18–20]. However, its effects on coordinated cellular pathways across different skin cell types and whether these cellular effects are associated with measurable changes in skin appearance remain incompletely characterized.

To address this gap, we used an integrated approach combining transcriptomic profiling, functional assays, and a controlled topical evaluation. Responses to EDL were characterized in primary human keratinocytes (NHEK) and dermal fibroblasts (HDF), examining pathways associated with proteostasis, antioxidant defense, inflammation, and senescence alongside functional measures of intracellular ROS, inflammatory cytokines, and senescence-associated β-galactosidase activity. A seven-flavonoid structure–function analysis was performed, with six additional flavonoids selected based on their relevance to polyphenol and skin research, to compare NRF2-associated gene expression and radical scavenging activity. Finally, changes in visible skin quality parameters following topical application of an EDL-containing formulation were evaluated over 12 weeks to determine whether cellular activities observed in vitro were accompanied by measurable skin-level outcomes.

2. Materials and Methods

2.1. Eriodictyol Active Ingredient

EDL (INCI: Eriodictyol, IUPAC: (2S)-2-(3,4-dihydroxyphenyl)-5,7-dihydroxy-3,4-dihydro-2H-1-benzopyran-4-one) was sourced from Debut Biotechnology, Inc. (Dermceutical EDL, San Diego, CA, USA) as a white powder with a purity of 92.7% (*w*/*w*) as determined by quantitative nuclear magnetic resonance. This ingredient was manufactured by fermentation using engineered *E. coli*, followed by proprietary downstream processing.

2.2. Cell Culture and Treatments

Primary NHEK cells (C-14002, PromoCell, Heidelberg, Germany) were grown in Keratinocyte Basal Medium 2 with Supplement Mix (C-20011, PromoCell), amphotericin B (AD0030P, Bio Basic, Markham, ON, Canada), and gentamicin (GB0217, Bio Basic). Primary HDF (C-013-5C, Thermo Fisher Scientific, Waltham, MA, USA) were grown in Fibroblast Basal Medium 2 (C-23020, PromoCell). Human immortalized keratinocytes (HaCaT) (AMS.iCell-h066-001b, Amsbio LLC, Cambridge, MA, USA) were cultured in DMEM (SH30243, Cytiva, Marlborough, MA, USA) containing 10% FBS (F0926, Sigma-Aldrich, St. Louis, MO, USA), 40 µg/mL amphotericin B (Bio Basic), and 0.05 µg/mL gentamicin (BioBasic) at 37 °C with 5% CO_2. Cells were expanded from cryopreserved stocks and maintained until cultures reached approximately 80% confluence. Primary cells were used for experiments at or before passage 3.

2.3. Cellular Viability

Cell viability was assessed using MTT or WST-8 colorimetric assays with commercially available kits following the manufacturer's protocols (MTT, #11465007001, Roche, Pleasanton, CA, USA; WST-8 #AB228554, Abcam, Cambridge, UK). Cells were seeded at 2.5×10^4 cells per well in clear, flat-bottom 96-well plates and allowed to adhere overnight. EDL was then applied at concentrations of 0–0.01% (0–347 µM) for 24 h. After treatment, cells were washed with phosphate-buffered saline (PBS) and incubated with the appropriate assay reagent. Absorbance was measured using a SpectraMax M5 plate reader (Molecular Devices, San Jose, CA, USA). Viability was expressed relative to cells treated with 0.1% DMSO vehicle.

2.4. RNA-Sequencing

2.4.1. Library Preparation and Sequencing

NHEK and HDF cells were grown as described above and treated with EDL (0.005% *w*/*w*, 173 µM), or 0.1% DMSO (Sigma-Aldrich) control for 24 h ($n = 3$). NHEK cells were treated with six additional flavonoids at the following concentrations for RNA sequencing: quercetin (0.005%), taxifolin (0.01%), catechin (0.005%), epicatechin (0.0003%), naringenin (0.0045%), dihydrokaempferol (0.003%) for 24 h, $n = 3$. Following treatment, mRNA was extracted from the cells using the Dynabeads mRNA Direct Kit (#61011, Thermo Fisher Scientific) according to the manufacturer's instructions. mRNA was further enriched via poly-A selection for library preparation (#334205, QIAGEN, Germantown, MD, USA). Prepared libraries were sequenced on an Illumina NextSeq 2000 platform (Illumina, San Diego, CA, USA) using paired-end sequencing (100 bp) with an average sequencing depth of 6 million reads per sample.

2.4.2. Transcriptomic Analysis

Sequencing reads were mapped to the human reference genome (GRCh38) and transcript (GENCODE v44) annotations using STAR v2.7.11a. Gene-level counts were generated

with featureCounts v2.0.6. Differential expression analysis was performed with DESeq2 v1.44.0; genes were considered differentially expressed at an adjusted $p \leq 0.05$ and an absolute $\log_2$ fold change > 0.5. KEGG pathway enrichment was assessed using gene set enrichment analysis (GSEA) method as implemented in ClusterProfiler v4.12.0. Selected pathways were visualized with Pathview v1.44.0, incorporating the corresponding gene-expression results.

2.5. Oxidative Stress Assays

2.5.1. Radical Scavenging

Antioxidant activity was evaluated using the ABTS radical cation decolorization assay as described with minor modifications [21]. The ABTS radical was generated by reacting 7 mM ABTS (HY-15902, MCE, Monmouth Junction, NJ, USA) with 2.45 mM ammonium persulfate (A3678, Sigma-Aldrich) in the dark at room temperature for 12–16 h, and then diluted to an absorbance of 0.70 ± 0.02 at 734 nm. Test articles were added to the working solution and incubated for 5 min at room temperature in the dark, after which absorbance was measured at 734 nm (SpectraMax M5, Molecular Devices).

DPPH radical scavenging was quantified by monitoring the decrease in absorbance following reaction with test articles. Fresh working solutions were prepared on the day of testing using 200 µM DPPH in ethanol (Cayman Chemical 14805, Ann Arbor, MI, USA), 400 µM Trolox (Cayman Chemical 10011659), for standard curve generation, and 0.01% (*w*/*w*) L-Ascorbic Acid as a positive control and ethanol was used as the negative control. Equal volumes of DPPH solution and test sample were mixed and incubated at 25 °C in the dark for 30 min. Absorbance was measured at 517 nm using a Spectramax M5 plate reader (Molecular Devices). Radical scavenging activity was expressed as percent inhibition relative to solvent control of $n = 3$ independent replicates.

2.5.2. Intracellular ROS (DCFDA)

To assess levels of cellular reactive oxygen species, a DCFDA/H2DCFDA-Cellular ROS Assay Kit (ab113851; Abcam) was used. In this assay, H2DCFDA reacts with intracellular ROS, producing a green fluorescence. To determine ROS levels in keratinocytes, HaCaT cells were cultured as described above. 1.5×10^4 cells were added to each well of a 96-well flat, clear-bottom, black microplate and allowed to adhere overnight. After overnight incubation, the media was aspirated, and cells were treated with test articles for 48 h. Following treatment, the media was aspirated, and cells were washed 1× with phosphate-buffered saline (PBS). Cells were then stained with 10 µM DCFDA in 1× assay buffer for 45 min at 37 °C. After staining, cells were washed and stimulated with 200 µM hydrogen peroxide (H_2O_2) in phenol red-free media for 30 min. After 30 min, fluorescence was measured with excitation at 485 nm and emission at 535 nm. Data are expressed as percent ROS relative to the DMSO vehicle control of $n = 3$ replicates.

2.6. Senescence-Associated β-Galactosidase (SA-β-Gal) Assay

HDF (Thermo Fisher Scientific) cells were cultured as described above and seeded at 10,000 cells/cm^2. Cells were maintained at 37 °C, 5% CO_2 for 24–48 h to allow attachment and stabilization. When confluency reached ~70–80%, culture medium was aspirated and replaced with fresh, pre-warmed medium containing 200 µM hydrogen peroxide (H_2O_2). After treating the cells for 2 h, the H_2O_2-containing culture medium was aspirated, and the cells were washed with Dulbecco's Phosphate-Buffered Saline (DPBS), which was then replaced with fresh, pre-warmed medium. Cells were incubated at 37 °C and 5% CO_2 for 48 h to allow recovery. Following the recovery period, HDF were treated with test articles diluted in culture medium and incubated for an additional 24 h. Cell number was then

determined using the CyQUANT Direct Red Cell Proliferation Kit (C35013, Thermo Fisher Scientific) according to the manufacturer's instructions. Culture medium was removed, cells were washed with DPBS, and SA-β-gal was analyzed according to the instructions outlined in the Senescence Detection Kit (ab65351, Abcam). After cell staining, microscopic images were captured using an ECHO Revolve microscope (ECHO, San Diego, CA, USA), and SA-β-gal activity was quantified by measuring the absorbance at 620 nm (corresponding to the absorbance maximum of the X-gal cleavage product) on a plate reader (SpectraMax M2, Molecular Devices). SA-β-gal absorbance was normalized to CyQUANT fluorescence in the same well. Data are $n \geq 3$ independent experiments. Statistical significance is relative to the DMSO + H_2O_2 control.

2.7. Anti-Inflammatory ELISA

The keratinocyte inflammatory-stimulation protocol was based on a previously published method, with measurement of IL-1β included alongside IL-6 for this study [22]. NHEK cells were seeded at 7500–10,000/cm^2 and maintained at 37 °C for 48–72 h before stimulation. The culture medium was then replaced with fresh, pre-warmed medium containing lipopolysaccharide (LPS, 2.0 µg/mL from *Escherichia coli* O26:B6, L8274, Sigma-Aldrich), and polyinosinic-polycytidylic acid (poly(I:C), 12.5 µg/mL, P1530, Sigma-Aldrich). After 1 h, test articles were added, and incubation continued for 24 h. Conditioned media were collected, and IL-6 and IL-1β concentrations were determined using ELISA kits (ELH-IL6 and ELH-IL1b, RayBiotech, Peachtree Corners, GA, USA) according to the manufacturer's instructions. Absorbance was measured using a SpectraMax M5 plate reader (Molecular Devices). Results are reported from $n = 3$ independent experiments. Statistical significance is relative to the DMSO + inflammatory cocktail-stimulated control.

2.8. Cosmetic Efficacy Study

2.8.1. Ethics and Informed Consent

This study protocol was reviewed and approved by the Allendale Institutional Review Board (AIRB, 30 Neck Road, Old Lyme, CT 06371, USA; Protocol DCS-22-25). Study conduct followed the Declaration of Helsinki, and principles of Good Clinical Practice requirements under Title 21 of the U.S. Code of Federal Regulations. Written informed consent form was obtained from all participants before any study procedure were undertaken.

2.8.2. Participant Criteria

Sixty healthy adult volunteers (82% female, 18% male) were enrolled in a randomized, double-blind, cosmetic efficacy study and were randomly assigned in equal numbers ($n = 30$ per group) to the active product or vehicle control group. The panel size was selected in line with enrollment typical for cosmetic efficacy studies of comparable design. Volunteers who provided informed consent and met all inclusion criteria and none of the exclusion criteria were enrolled at the baseline visit.

Inclusion Criteria

Eligible participants were female and male volunteers with mild to moderate photodamage (3–6 Griffith's Scale), 30–75 years of age, with Fitzpatrick skin types I-VI. Volunteers were in general good health with no known conditions that, in the grader's opinion, might interfere with the study, and agreed to use the assigned test sample along with the provided SPF for the study duration.

Exclusion Criteria

Volunteers were excluded if they had severe photoaged appearance, regular use of artificial light sources or tanning booths, worked outdoors or had excessive sunlight exposure, had any skin condition that might interfere with the assessments, used topical prescription or OTC facial products within 2 weeks before study entry, or professional treatments within 6 months before the study.

2.8.3. Design and Assessments

Enrolled volunteers were randomized to either the active product, containing 0.5% *w*/*w* EDL, or the vehicle control group. Each base formulation was identical apart from EDL and contained Water (Aqua/Eau), Dimethyl Isosorbide, Hydrogenated Farnesene, Butylene Glycol, Glycerin, Glyceryl Stearate SE, *Helianthus annuus* (Sunflower) Seed Oil, Sodium Acrylates Copolymer, Cetyl Alcohol, Hydroxyacetophenone, Caprylyl Glycol, 1,2-Hexanediol, and Lecithin. Each test product was applied to the entire face immediately following skin cleansing twice daily (morning and night), and application was verified by a compliance journal. Morning applications were followed by an SPF product.

Assessments were performed at baseline and at weeks 4, 8, and 12 on clean, dry skin. Results are reported at week 12, the pre-specified primary time point. Facial attributes were graded by a trained expert investigator on a 5-point ordinal scale (0 = none, 1 = minimal, 2 = mild, 3 = moderate, 4 = severe) for poor visual texture, poor tactile texture, wrinkles, fine lines, uneven skin tone, lack of luminosity, skin sagging, lack of elasticity, and overall photodamage. Standardized photographs (VISIA, Standard 1 lighting, Canfield Scientific, Parsippany, NJ, USA) were captured at each visit for documentation only and were not used for grading.

2.9. Statistical Analysis

Statistical analyses were performed using JMP Pro 19. Data are reported as mean ± standard deviation unless otherwise indicated. Concentration-dependent effects were evaluated by nonlinear regression using a sigmoidal dose–response model to estimate IC_{50} values. In vitro experiment group comparisons were performed using one-way analysis of variance (ANOVA) followed by Dunnett's post hoc test, comparing treatments with the appropriate control. For clinical outcomes, within-group changes from baseline were analyzed using the Wilcoxon signed-rank test, and between-group differences in change from baseline were analyzed using the Mann–Whitney U test. Clinical *p*-values were adjusted across the nine graded attributes using the Benjamini–Hochberg false discovery rate procedure. Statistical significance was defined as adjusted $p < 0.05$.

2.10. Artificial Intelligence Use

The authors used generative artificial intelligence tools to support manuscript organization, language refinement, and readability. The authors critically reviewed and revised all text and accept full responsibility for the accuracy and integrity of the final manuscript.

3. Results

3.1. EDL Elicits Broad Transcriptomic Changes in Keratinocytes and Dermal Fibroblasts

The cytotoxic potential of EDL was first evaluated in fibroblasts and keratinocytes using an MTT viability assay (Figure S1). Across the concentration range tested, EDL maintained cell viability above the predefined 80% threshold, establishing 0.005% (~173 µM) as the concentration used for transcriptomic analysis. At this concentration, EDL altered gene expression in both HDF and NHEK (Figure 1a,b). Differential expression analysis identified

3589 differentially expressed genes (DEGs) in NHEK, (1600 upregulated, 1989 downregulated) and 3073 DEGs in HDF (1374 upregulated, 1699 downregulated). Apoptosis, necroptosis, and p53 signaling pathways were mostly reduced. Caspase-associated pathways were likewise not enriched.

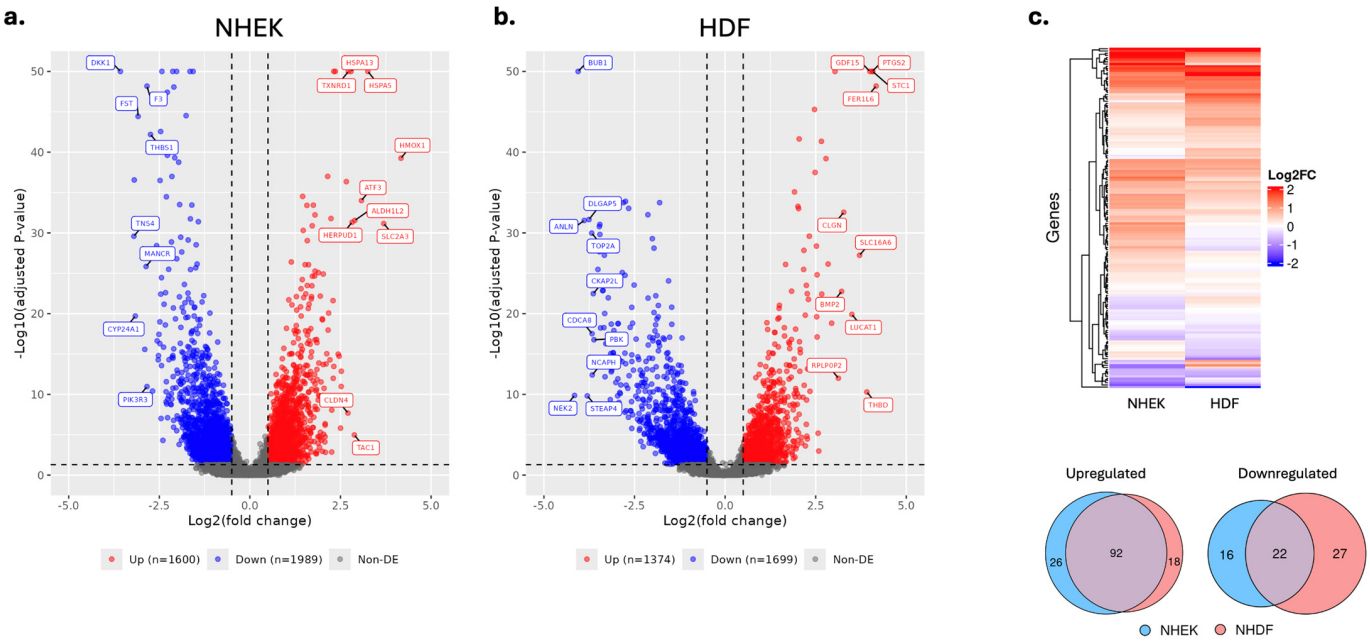


Figure 1. Transcriptome responses to EDL in primary skin cells. (**a**,**b**) Volcano plots showing the gene expression profile after 24-h EDL exposure in NHEK (**a**) and HDF (**b**). Differential expression (DE) is defined by adjusted p-value < 0.05 and absolute log2(fold change) > 0.5, indicated by the dashed lines. Up- and down-regulated DE genes are shown in red and blue, respectively. The top 10 most strongly regulated genes are labeled. (**c**) Heatmap of 156 genes in the "Protein Processing in the ER" KEGG pathway that are expressed in both cell types (**top**). Venn diagrams show overlap among up- and down-regulated genes in the "Protein processing in ER" KEGG pathway across cell types (**bottom**).

Despite distinct transcriptomic profiles, both cell types exhibited enrichment of UPR-associated genes (Figure 1c). Expression increased for ER chaperones and protein-folding genes, including *HSPA5* (BiP), *HYOU1* (GRP170), *DNAJB9*, *HERPUD1*, *CALR*, and *CANX*, together with ER stress sensors *ERN1* (IRE1a) and *EIF2AK3* (PERK). Downstream integrated stress response genes, including *ATF3*, *ATF4*, and *DDIT3* (CHOP), were also increased. GSEA of 228 KEGG pathways showed "Protein processing in the endoplasmic reticulum" as a highly enriched pathway in both cell types.

3.2. EDL Regulates NRF2-Associated Antioxidant and Autophagy-Related Transcriptional Pathways in Keratinocytes

Building on the global transcriptional changes observed above (Section 3.1), we next examined keratinocyte-specific pathways regulated by EDL. EDL induced an NRF2/ARE antioxidant gene signature, with *HMOX1* as the most strongly upregulated transcript (log2FC +4.17, ~17.5-fold). Additional canonical NRF2 target were significantly induced, including *TXNRD1* (+2.72), *GCLM* (+2.36), *SLC7A11* (+2.00), *GCLC* (+1.89), and *SESN2* (+1.20) (Figures 2b and S4b). These genes span multiple NRF2-regulated antioxidant systems, including heme degradation, thioredoxin recycling, glutathione biosynthesis, and cystine transport.

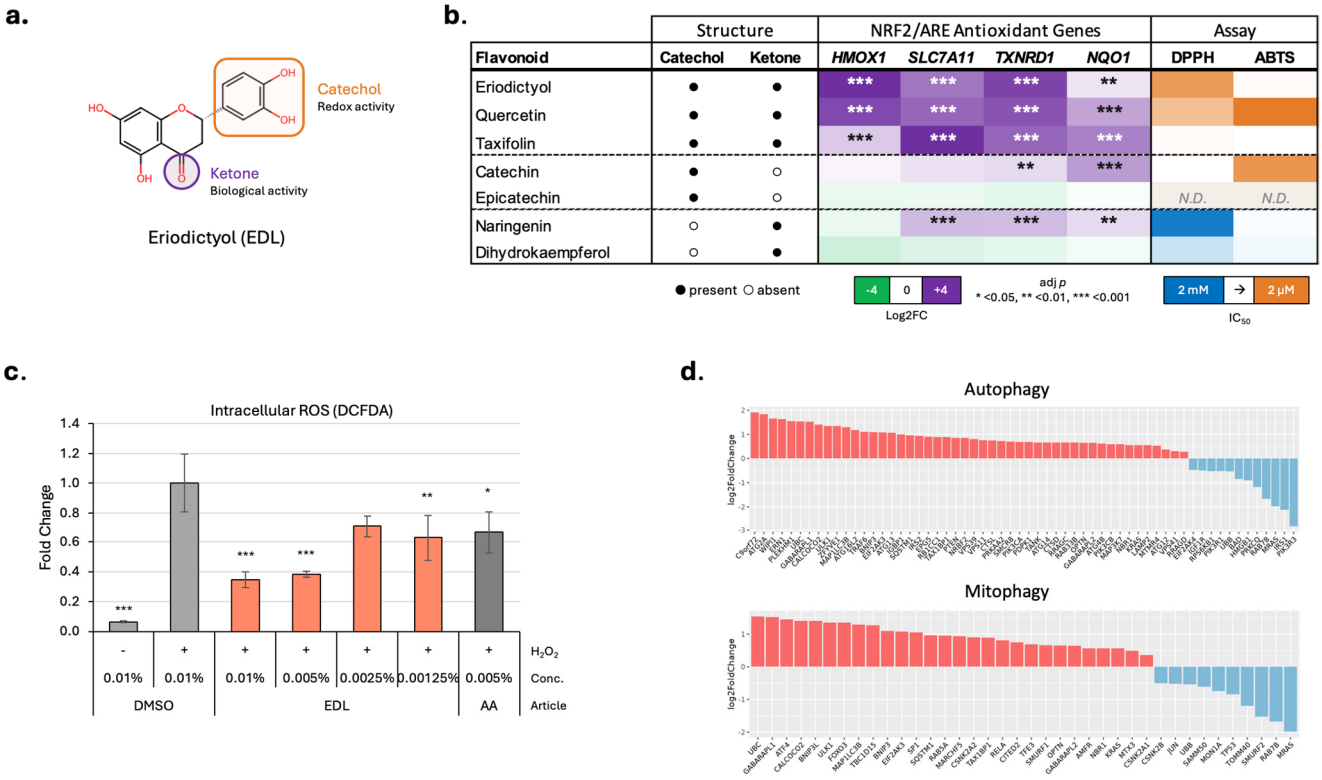


Figure 2. Structural features of EDL and their relationship to antioxidant activity and cytoprotective responses. (**a**) The structure of EDL highlights the catechol B-ring and C4 ketone. (**b**) A summary of a flavonoid structure-activity comparison across seven compounds in NHEK, with the structural features, selected NRF2-associated gene expression Log2 fold change (green (decreased) to purple (increased) color), statistical significance (asterisks), and activities in two radical-scavenging assays (blue to orange color). Additional data are available in Figure S4. (**c**) Intracellular ROS measured by DCFDA assay in HaCaT cells following 48 h pre-treatment with DMSO (light grey), EDL (orange), and ascorbic acid (AA, dark grey), and subsequent stimulation by H_2O_2. ROS fold change relative to DMSO is plotted against test articles, concentrations, and the presence of H_2O_2. * $p < 0.05$, ** $p < 0.01$, *** $p < 0.001$ (**d**) Expression changes in NHEK genes in the Autophagy and Mitophagy KEGG pathways, limited to those with adjusted p-value < 0.05.

To identify the structural features associated with NRF2 activation, we compared EDL with six related flavonoids using RNA-sequencing in NHEK cells (Figures 2b and S4). Strong activation of the NRF2/ARE gene signature was observed only in flavonoids containing both a 3′4′-catechol B-ring and a C-ring 4-ketone. EDL, quercetin, and taxifolin, which contain both features, showed the greatest induction across the NRF2/ARE panel, whereas catechol-containing flavan-3-ols lacking the 4-ketone (catechin and epicatechin) and non-catechol flavanones (naringenin and dihydrokaempferol) showed little or no activity. This structure-activity relationship was further illustrated by two matched scaffold pairs in which the addition of the 3′-hydroxyl group converted weakly active flavonoids into NRF2/ARE inducers (Figure S4).

EDL also demonstrated radical scavenging capacity in acellular ABTS and DPPH assays ($IC_{50} \approx 0.0006\%$ and 0.0002% w/w, respectively; Figure S4). Consistent with these findings, EDL produced a dose-dependent reduction in H_2O_2-induced intracellular ROS in immortalized keratinocytes measured by a DCFDA assay (Figure 2c, Table S1). At the concentrations tested, the reduction in intracellular ROS was comparable to that observed with 0.005% (~284 µM) ascorbic acid, with the highest EDL concentrations producing similar or greater reductions relative to the oxidative stress control.

In addition to NRF2-associated antioxidant genes, EDL regulated autophagy-related transcriptional pathways in keratinocytes (Figures 2d, S5 and S6). GSEA identified enrichment of autophagy (NES = +1.83), mitophagy (+1.78), and lysosome (+1.96) pathways compared to vehicle control (Figure S2). Gene-level changes included expression of genes associated with autophagy initiation (*ULK1*, +1.35), autophagosome formation (*MAP1LC3B*, +1.29), and mitochondrial targeting (*BNIP3L*, +1.40; *BNIP3*, +1.10). Upstream regulatory analysis further identified increased *FOXO3* (+1.35) expression, consistent with regulation of autophagy-associated transcriptional pathways (Figure S5). Lysosome pathway enrichment was observed in NHEK but not HDF, indicating preferential enrichment in keratinocytes.

3.3. EDL Regulates Inflammatory Signaling and Senescence-Associated Pathways

Inflammatory signaling and cellular senescence are important features of age-associated skin dysfunction. We next examined inflammatory signaling and senescence-associated endpoints in keratinocytes and dermal fibroblasts. EDL reduced inflammatory gene expression in both cell types and altered pathways associated with proliferation, metabolism, and senescence in dermal fibroblasts (Figure 3).

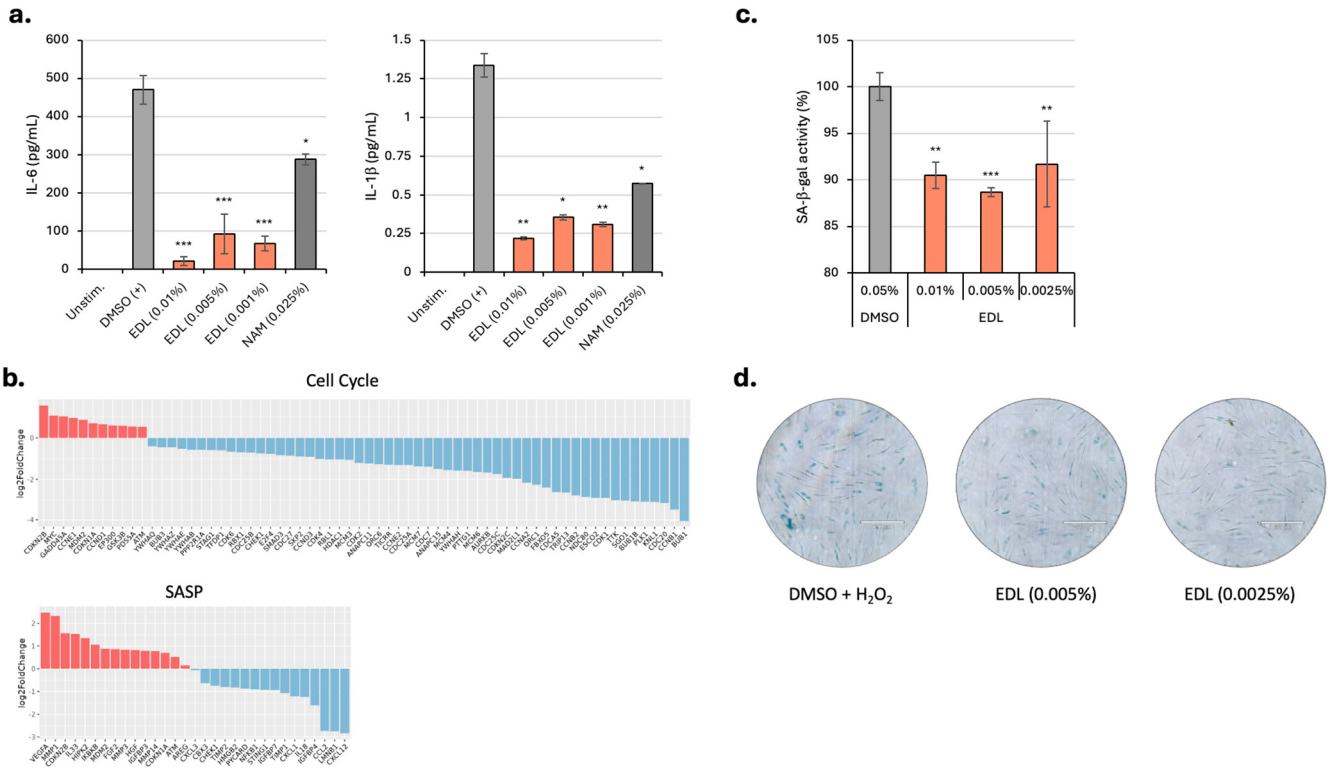


Figure 3. Modulation of inflammatory signaling, senescence-associated gene expression, and SA-β-gal activity by EDL. (**a**) Pro-inflammatory cytokine secretion in NHEK measured by ELISA. Extracellular IL-6 (**left**) and IL-1β (**right**) levels were quantified by ELISA following treatment with the indicated concentration of test article in the presence of LPS + poly(I:C) stimulation. (**b**) Expression change in HDF genes in either the Cell Cycle KEGG pathway or known to be part of the SASP response, limited to those with adjusted *p*-value < 0.05. Genes with positive and negative fold changes are shown in red and blue, respectively (**c**,**d**) SA-β-gal activity in HDF in response to EDL treatment. (**c**) Quantification of SA-β-gal activity expressed as percent activity relative to the DMSO + H_2O_2 control. Cells were treated with EDL ranging from 0.0001–0.005%. (**d**) Representative bright-field images of SA-β-gal-stained cells from the control and the two statistically significant EDL groups. Senescent cells that stain positive for SA-β-gal activity are identified by blue cytoplasmic coloration. Scale bar = 670 µm. * $p < 0.05$, ** $p < 0.01$, *** $p < 0.001$.

In keratinocytes, EDL reduced expression of genes associated with NF-kB signaling, including *IL-1b* (−1.05), *CXCL1* (−2.48), and *NFKB1* (−0.78). Gene Ontology analysis of cytokine activity showed increased expression of *GDF15*, *VEGFA,* and *TIMP1,* along with reduced expression of several pro-inflammatory mediators (Figure S6). These transcriptional changes were accompanied by reduced cytokine secretion following LPS and poly(I:C) stimulation (Figure 3a). EDL tested at 0.001%, 0.005%, and 0.01% significantly reduced IL-6 secretion by 72–87% relative to the DMSO control ($p < 0.001$). IL-1β secretion was also reduced at all three concentrations, by 81% ($p = 0.009$), 67% ($p = 0.012$), and 88% ($p = 0.008$), respectively.

In dermal fibroblasts, EDL altered pathways associated with proliferation and metabolism, with DNA replication (−2.36) and cell cycle (−2.40) among the most downregulated KEGG pathways (Figure S3). Consistent with these pathway-level changes, *BUB1* (Log2FC −4.06), *CCNB1* (−3.47), and *CDC20* (−3.15) genes involved in mitotic checkpoint regulation were among the most strongly downregulated transcripts (Figure 3b).

EDL additionally altered the expression of genes associated with inflammatory signaling and SASP in HDF. Expression of *CCL2* (−2.73), *CXCL1* (−1.21), *IL-18* (−1.24), and *NFKB1* (−0.90) decreased, whereas *GDF15* (+4.00) increased. To test whether these transcriptional changes translated into functional effects on senescence-associated phenotypes, we induced senescence in dermal fibroblasts with hydrogen peroxide and subsequently exposed them to EDL. After normalizing to cell number, EDL significantly reduced senescence-associated β-galactosidase activity relative to the DMSO + H_2O_2 control at all concentrations tested; by 8.3% at 0.0025% EDL ($p = 0.008$), 11.3% at 0.005% EDL ($p < 0.001$), and 9.5% at 0.01% EDL ($p = 0.002$) (Figure 3c). Representative images showed fewer SA-β-gal-positive cells at these concentrations (Figure 3d).

3.4. Effects of Topical EDL on Visible Skin Quality

To evaluate the effects of topical EDL on visible skin quality, a randomized, double-blind, vehicle-controlled cosmetic evaluation study was conducted over 12 weeks ($n = 30$ per group). Nine attributes were graded by a trained expert at baseline and after 4, 8, and 12 weeks of twice-daily use. No adverse events were reported, and the study met predefined tolerability and safety criteria.

At week 12, EDL produced significantly greater improvements than vehicle in visual texture, fine lines, luminosity, sagging, and overall photodamage (adjusted $p < 0.05$; Table 1, Figure 4a). Fine lines, sagging, and overall photodamage improved from baseline only with EDL. Elasticity and tone also improved from baseline with EDL only, although the differences versus vehicle were not significant. Visual texture and luminosity improved in both groups, but improvements were approximately twofold greater with EDL (34% vs. 19% and 34% vs. 16%, respectively). Tactile texture improved similarly in both groups, and wrinkles did not change. Representative images are shown in Figure 4b (EDL) and Figure S7 (vehicle). The greater improvements observed with EDL compared with vehicle at week 12 for multipole attributes suggest an EDL-associated effect.

Table 1. Cosmetic efficacy study outcomes at week 12.

Attribute	EDL Baseline	EDL Change (%)	V Baseline	V Change (%)	EDL vs. V adj. *p*
Visual Texture	2.67 ± 0.48	−0.90 ± 0.40 (−34%) **	2.67 ± 0.48	−0.50 ± 0.51 (−19%) **	**0.005**
Tactile Texture	2.63 ± 0.49	−0.90 ± 0.40 (−34%) **	2.67 ± 0.48	−0.73 ± 0.58 (−28%) **	0.22
Wrinkles	2.73 ± 0.52	−0.07 ± 0.25 (−2%)	2.70 ± 0.47	0.00 ± 0.00 (0%)	0.24
Fine Lines	2.77 ± 0.50	−0.33 ± 0.48 (−12%) **	2.73 ± 0.45	0.00 ± 0.00 (0%)	**<0.003**
Tone	2.70 ± 0.53	−0.20 ± 0.41 (−7%) *	2.80 ± 0.55	−0.13 ± 0.35 (−5%)	0.50
Luminosity	2.73 ± 0.45	−0.93 ± 0.52 (−34%) **	2.70 ± 0.47	−0.43 ± 0.50 (−16%) **	**<0.003**

Table 1. *Cont.*

Attribute	EDL Baseline	EDL Change (%)	V Baseline	V Change (%)	EDL vs. V adj. *p*
Sagging	2.73 ± 0.45	−0.37 ± 0.49 (−13%) **	2.67 ± 0.48	−0.10 ± 0.31 (−4%)	**0.03**
Elasticity	2.63 ± 0.49	−0.30 ± 0.47 (−11%) **	2.63 ± 0.49	−0.07 ± 0.37 (−3%)	0.06
Overall	2.77 ± 0.43	−0.60 ± 0.56 (−22%) **	2.77 ± 0.43	−0.17 ± 0.38 (−6%)	**<0.003**

Mean ± SD (% change); $n = 30$ per group. V, vehicle. Attributes expertly graded as severity (e.g., lack of luminosity, uneven tone); negative change indicates improvement. Within-group change from baseline: Wilcoxon signed-rank, * $p < 0.05$, ** $p < 0.01$. Between-group differences: Mann–Whitney U, *p*-values Benjamini–Hochberg-adjusted across nine attributes; bold $p < 0.05$.

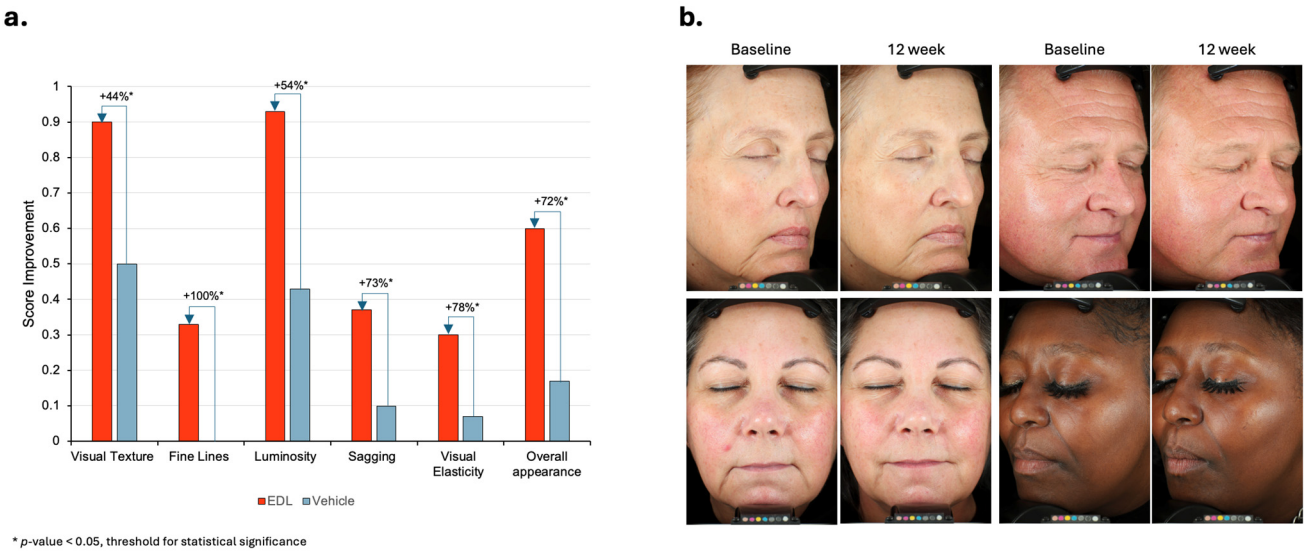


Figure 4. Evaluation of topical EDL on facial aging parameters. (**a**) Summary of baseline to week 12 improvements in skin attributes for EDL and the vehicle control groups ($n = 30$ each) with differences between groups shown as percent improvement and significance indicated by asterisks. Arrows indicate the bars (EDL) that increase relative to the reference (Vehicle) for each attribute. (**b**) Representative EDL product application participants at baseline and 12-week timepoints demonstrating improvements in the appearance of marionette lines, fine lines and wrinkles, and skin luminosity. Vehicle control participants are shown in Figure S7. * *p*-value < 0.05 threshold for statistical significance.

4. Discussion

Taken together, EDL elicited a shared stress-adaptive signature across keratinocytes and dermal fibroblasts while producing distinct cell-type-specific changes. Both cell types showed activation of the unfolded protein response, without evidence of cytotoxicity. This pattern is consistent with engagement of interconnected ER stress-sensing and antioxidant defense pathways, including PERK- and NRF2-associated signaling. At the same time, the transcriptional profiles retained clear differences between epidermal and dermal cells, with keratinocytes showing stronger antioxidant and autophagy-related activity and fibroblasts showing changes in proliferative, metabolic, and senescence-associated pathways.

In keratinocytes, EDL induced NRF2-associated antioxidant responses together with enrichment of autophagy, mitophagy, and lysosomal pathways, suggesting potential regulation of cellular quality control, proteostasis, and mitochondrial function. Keratinocyte autophagy contributes to barrier maintenance, inflammatory regulation, and adaptation to environmental stress [23,24]. Disruption of epidermal autophagy can also alter fibroblast activation and dermal repair responses through paracrine signaling, suggesting that changes induced in keratinocytes may influence broader skin homeostasis [25]. These processes may contribute to the improvements in skin texture and luminosity observed clinically.

Fibroblasts responded differently from keratinocytes, showing reduced proliferative and metabolic pathway activity and attenuated inflammatory and senescence-associated signatures. Reduced SA-β-galactosidase activity and cytokine release support a senomorphic response rather than induction of classical senescence. Similar regulation of oxidative stress and SASP-associated pathways has been reported for other NRF2-associated phytochemicals, including cistanche-derived polysaccharides and galangin, placing EDL within a broader group of compounds that regulate aging-associated inflammatory phenotypes while maintaining cellular viability [26,27].

The observed changes in skin appearance complement the cellular responses identified in vitro (Figure 5). The interaction between the epidermal and dermal compartments are central to skin aging, with oxidative stress, inflammatory signaling, and extracellular matrix alterations contributing to reciprocal changes between keratinocytes and fibroblasts [28]. Reduced oxidative and inflammatory signaling in keratinocytes, together with modulation of fibroblast senescence-associated responses, provide potential biological context for the improvements in texture, luminosity, elasticity, and sagging observed during topical evaluation. However, molecular biomarkers were not assessed in participants, and EDL skin penetration was not measured. The in vitro concentrations were selected based on an approximate 1% skin-delivery assumption, consistent with reported median epidermal recovery for cosmetic-related chemicals [29]. Because skin penetration varies by compound, the concentration of EDL reaching viable skin following topical application is unknown. Direct relationships between EDL exposure, specific cellular pathways, and observable outcomes remain to be established.

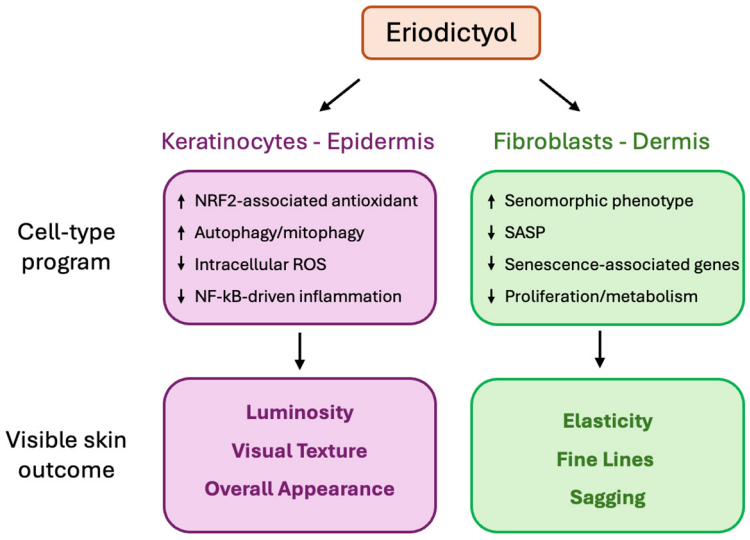


Figure 5. Proposed mechanisms for EDL activity in skin. EDL induces an NRF2-associated antioxidant and anti-inflammatory program in keratinocytes and a senomorphic, quiescent-like program in dermal fibroblasts. These cell-type-specific responses are consistent with improvements in skin appearance, although direct molecular links were not assessed in the study participants' samples.

The seven-flavonoid structure-function analysis further contextualized EDL within the broader flavonoid family (Figures 2 and S4). These findings indicate that NRF2 pathway activation was associated with specific structural features rather than radical scavenging capacity alone. Although catechol-containing flavonoids showed comparable activity in chemical radical-scavenging assays, EDL produced the strongest induction of several NRF2-associated genes, consistent with previous studies in other cell types [30,31]. These data suggest that the biological activity of EDL is linked to engagement of endogenous antioxidant defense pathways in addition to its intrinsic chemical properties.

EDL joins a list of flavonoids that can engage NRF2-associated protective responses in skin [32]. Previous studies demonstrated EDL activity in NRF2-dependent fibroblast protection and modulation of UV-associated signaling in keratinocytes [18,20]. The current study extends these observations by characterizing EDL responses at the transcriptome-wide level in both keratinocytes and dermal fibroblasts, supported by functional validation and a vehicle-controlled human evaluation. Future studies using co-culture or organotypic 3D skin models could further examine interactions between these cell types. Longer-term evaluations incorporating skin penetration studies and serial biomarker assessments could clarify the persistence of EDL-associated effects and determine whether the pathways identified in vitro are also modulated in human skin.

5. Conclusions

This study integrates transcriptomic profiling, functional assays, and vehicle-controlled human evaluation to characterize the biological activity of EDL across major skin cell types. In vitro, EDL modulates cell-type-specific antioxidant, inflammatory, and proteostasis pathways in keratinocytes and dermal fibroblasts and reduces senescence-associated markers in fibroblasts. In the 12-week topical evaluation, EDL significantly improved multiple measures of visible skin quality compared with vehicle. These findings support further investigation of EDL as a topical ingredient for skin aging.

Supplementary Materials: The following supporting information can be downloaded at: https://www.mdpi.com/article/10.3390/antiox15111444/s1, Figure S1: Cellular viability assays; Figure S2: EDL-modulated KEGG pathway gene expression analysis in NHEK; Figure S3: EDL-modulated KEGG pathway gene expression analysis in HDF; Figure S4: Structure-function studies of seven flavonoids; Figure S5: EDL upregulates homeostasis programs in NHEK; Figure S6: Pathway-level gene expression analysis following EDL treatment in NHEK; Figure S7: Representative vehicle participants at baseline and 12-week timepoints; Table S1: Statistical summary of EDL concentration-dependent inhibition of oxidative stress, cellular senescence, and pro-inflammatory cytokine secretion.

Author Contributions: Conceptualization, T.O. and N.J.B.; investigation, Z.S., D.Z., J.M.F. and E.B.L.; software, Z.S.; formal analysis, T.O., Z.S. and N.J.B.; writing—original draft preparation, N.J.B.; writing—review and editing, T.O., Z.S. and N.J.B.; visualization, T.O., Z.S. and N.J.B.; supervision, T.O. and N.J.B.; All authors have read and agreed to the published version of the manuscript.

Funding: This research received no external funding.

Institutional Review Board Statement: The study was conducted in accordance with the Declaration of Helsinki, and approved by the Allendale Institutional Review Board (AIRB, 30 Neck Road, Old Lyme, CT 06371, USA) Protocol DCS-22-25, approved 8 September 2025.

Informed Consent Statement: Informed consent was obtained from all participants involved in the study. Written informed consent has been obtained from all participants in this study to publish this paper.

Data Availability Statement: The original contributions presented in this study are included in the article. Additional datasets referenced in this study are available upon reasonable request from the corresponding author due to their confidential and proprietary nature.

Acknowledgments: The authors would like to thank all participants, Zoe Draelos, and Dermatology Consulting Services, PLLC, for their assistance in this cosmetic study.

Conflicts of Interest: T.O., Z.S., D.Z., J.M.F., E.B.L., and N.J.B. are employees of Debut Biotechnology, Inc. T.O. is a named inventor on a patent related to this work, which is solely owned by Debut Biotechnology, Inc. Debut Biotechnology, Inc. supplied the test ingredient and was involved in study design, data analysis, data interpretation, and manuscript preparation. The remaining authors declare that the research was conducted in the absence of any commercial or financial relationships that could be construed as a potential conflict of interest.

Abbreviations

The following abbreviations are used in this manuscript:

CFR	Code of federal regulations
DMSO	Dimethyl sulfoxide
DNA	Deoxyribonucleic acid
ECM	Extracellular matrix
EDL	Eriodictyol
ELISA	Enzyme-linked immunosorbent assay
ER	Endoplasmic reticulum
GOBP	Gene ontology biological process
GSEA	Gene set enrichment analysis
H_2O_2	Hydrogen peroxide
HDF	Human dermal fibroblasts
IL-1β	Interleukin-1 beta
IL-6	Interleukin-6
KEGG	Kyoto encyclopedia of genes and genomes
LPS	Lipopolysaccharide
MMP	Matrix metalloproteinase
mRNA	Messenger ribonucleic acid
MTT	3-(4,5-dimethylthiazol-2-yl)-2,5-diphenyltetrazolium bromide
NHEK	Normal human epidermal keratinocytes
PBS	Phosphate-buffered saline
ROS	Reactive oxygen species
SASP	Senescence-associated secretory phenotype
UPR	Unfolded protein response

References

1. Rinnerthaler, M.; Bischof, J.; Streubel, M.; Trost, A.; Richter, K. Oxidative Stress in Aging Human Skin. *Biomolecules* **2015**, *5*, 545–589. [CrossRef] [PubMed]
2. Lee, H.; Hong, Y.; Kim, M. Structural and Functional Changes and Possible Molecular Mechanisms in Aged Skin. *Int. J. Mol. Sci.* **2021**, *22*, 12489. [CrossRef] [PubMed]
3. Quan, T.; Fisher, G.J. Role of Age-Associated Alterations of the Dermal Extracellular Matrix Microenvironment in Human Skin Aging: A Mini-Review. *Gerontology* **2015**, *61*, 427–434. [CrossRef] [PubMed]
4. Nan, L.; Guo, P.; Hui, W.; Xia, F.; Yi, C. Recent Advances in Dermal Fibroblast Senescence and Skin Aging: Unraveling Mechanisms and Pioneering Therapeutic Strategies. *Front. Pharmacol.* **2025**, *16*, 1592596. [CrossRef] [PubMed]
5. Zheng, J.; Wang, S.; Sun, J.; Lv, J. Dermal Fibroblast Senescence: The Central Hub of Skin Aging—From Intrinsic Dysfunction to Microenvironmental Remodeling. *Int. J. Mol. Sci.* **2026**, *27*, 1653. [CrossRef] [PubMed]
6. Motohashi, H.; Yamamoto, M. Nrf2–Keap1 Defines a Physiologically Important Stress Response Mechanism. *Trends Mol. Med.* **2004**, *10*, 549–557. [CrossRef] [PubMed]
7. Boo, Y.C. Natural Nrf2 Modulators for Skin Protection. *Antioxidants* **2020**, *9*, 812. [CrossRef] [PubMed]
8. Hetz, C.; Zhang, K.; Kaufman, R.J. Mechanisms, Regulation and Functions of the Unfolded Protein Response. *Nat. Rev. Mol. Cell Biol.* **2020**, *21*, 421–438. [CrossRef] [PubMed]
9. Cullinan, S.B.; Zhang, D.; Hannink, M.; Arvisais, E.; Kaufman, R.J.; Diehl, J.A. Nrf2 Is a Direct PERK Substrate and Effector of PERK Dependent Cell Survival. *Mol. Cell Biol.* **2003**, *23*, 7198–7209. [CrossRef] [PubMed]
10. Cullinan, S.B.; Diehl, J.A. PERK-Dependent Activation of Nrf2 Contributes to Redox Homeostasis and Cell Survival Following Endoplasmic Reticulum Stress. *J. Biol. Chem.* **2004**, *279*, 20108–20117. [CrossRef] [PubMed]
11. Izzi, V. The Effects of Dietary Flavonoids on the Regulation of Redox Inflammatory Networks. *Front. Biosci.* **2012**, *17*, 2396–2418. [CrossRef] [PubMed]
12. Jomova, K.; Alomar, S.Y.; Valko, R.; Liska, J.; Nepovimova, E.; Kuca, K.; Valko, M. Flavonoids and Their Role in Oxidative Stress, Inflammation, and Human Diseases. *Chem. Biol. Interact.* **2025**, *413*, 111489. [CrossRef] [PubMed]
13. Rattan, S. Hormetins as Novel Components of Cosmeceuticals and Aging Interventions. *Cosmetics* **2015**, *2*, 11–20. [CrossRef]
14. Rattan, S.I.S.; Kryzch, V.; Schnebert, S.; Perrier, E.; Nizard, C. Hormesis-Based Anti-Aging Products: A Case Study of a Novel Cosmetic. *Dose-Response* **2012**, *11*, 99–108. [CrossRef] [PubMed]
15. Islam, A.; Islam, M.S.; Rahman, M.K.; Uddin, M.N.; Akanda, M.R. The Pharmacological and Biological Roles of Eriodictyol. *Arch. Pharm. Res.* **2020**, *43*, 582–592. [CrossRef] [PubMed]

16. Deng, Z.; Hassan, S.; Rafiq, M.; Li, H.; He, Y.; Cai, Y.; Kang, X.; Liu, Z.; Yan, T. Pharmacological Activity of Eriodictyol: The Major Natural Polyphenolic Flavanone. *Evid.-Based Complement. Altern. Med.* **2020**, *2020*, 6681352. [CrossRef] [PubMed]
17. Yin, H.; Li, Y.; Feng, Y.; Tian, L.; Li, Y. The Extraction, Biosynthesis, Health-Promoting and Therapeutic Properties of Natural Flavanone Eriodictyol. *Nutrients* **2024**, *16*, 4237. [CrossRef] [PubMed]
18. Nisar, M.F.; Liu, T.; Wang, M.; Chen, S.; Chang, L.; Karisma, V.W.; Weixu; Diao, Q.; Xue, M.; Tang, X.; et al. Eriodictyol Protects Skin Cells from UVA Irradiation-Induced Photodamage by Inhibition of the MAPK Signaling Pathway. *J. Photochem. Photobiol. B* **2022**, *226*, 112350. [CrossRef] [PubMed]
19. Lee, E.-R.; Kim, J.-H.; Kang, Y.-J.; Cho, S.-G. The Anti-Apoptotic and Anti-Oxidant Effect of Eriodictyol on UV-Induced Apoptosis in Keratinocytes. *Biol. Pharm. Bull.* **2007**, *30*, 32–37. [CrossRef] [PubMed]
20. Lee, E.-R.; Kim, J.-H.; Choi, H.Y.; Jeon, K.; Cho, S.-G. Cytoprotective Effect of Eriodictyol in UV-Irradiated Keratinocytes via Phosphatase-Dependent Modulation of Both the P38 MAPK and Akt Signaling Pathways. *Cell. Physiol. Biochem.* **2011**, *27*, 513–524. [CrossRef] [PubMed]
21. Re, R.; Pellegrini, N.; Proteggente, A.; Pannala, A.; Yang, M.; Rice-Evans, C. Antioxidant Activity Applying an Improved ABTS Radical Cation Decolorization Assay. *Free Radic. Biol. Med.* **1999**, *26*, 1231–1237. [CrossRef] [PubMed]
22. Oswald, T.; Shao, Z.; Zambrano, D.; Brideau, N.J. Dihydrokaempferol Supports Epidermal Barrier, Dermal Repair, and Enhances Post-Procedure Recovery. *Cosmetics* **2026**, *13*, 93. [CrossRef]
23. Giroud, J.; Combémorel, E.; Pourtier, A.; Abbadie, C.; Pluquet, O. Unraveling the Functional and Molecular Interplay between Cellular Senescence and the Unfolded Protein Response. *Am. J. Physiol. Cell Physiol.* **2025**, *328*, C1764–C1782. [CrossRef] [PubMed]
24. Liu, C.; Gu, L.; Ding, J.; Meng, Q.; Li, N.; Dai, G.; Li, Q.; Wu, X. Autophagy in Skin Barrier and Immune-Related Skin Diseases. *J. Dermatol.* **2021**, *48*, 1827–1837. [CrossRef] [PubMed]
25. Qiang, L.; Yang, S.; Cui, Y.-H.; He, Y.-Y. Keratinocyte Autophagy Enables the Activation of Keratinocytes and Fibroblastsand Facilitates Wound Healing. *Autophagy* **2020**, *17*, 2128–2143. [CrossRef] [PubMed]
26. Takaya, K.; Asou, T.; Kishi, K. Cistanche Deserticola Polysaccharide Reduces Inflammation and Aging Phenotypes in the Dermal Fibroblasts through the Activation of the NRF2/HO-1 Pathway. *Int. J. Mol. Sci.* **2023**, *24*, 15704. [CrossRef] [PubMed]
27. Lee, J.-J.; Ng, S.-C.; Hsu, J.-Y.; Liu, H.; Chen, C.-J.; Huang, C.-Y.; Kuo, W.-W. Galangin Reverses H2O2-Induced Dermal Fibroblast Senescence via SIRT1-PGC-1α/Nrf2 Signaling. *Int. J. Mol. Sci.* **2022**, *23*, 1387. [CrossRef] [PubMed]
28. Zhang, J.; Yu, H.; Man, M.-Q.; Hu, L. Aging in the Dermis: Fibroblast Senescence and Its Significance. *Aging Cell* **2023**, *23*, e14054. [CrossRef] [PubMed]
29. Hewitt, N.J.; Grégoire, S.; Cubberley, R.; Duplan, H.; Eilstein, J.; Ellison, C.; Lester, C.; Fabian, E.; Fernandez, J.; Géniès, C.; et al. Measurement of the Penetration of 56 Cosmetic Relevant Chemicals into and through Human Skin Using a Standardized Protocol. *J. Appl. Toxicol.* **2019**, *40*, 403–415. [CrossRef] [PubMed]
30. Johnson, J.; Maher, P.; Hanneken, A. The Flavonoid, Eriodictyol, Induces Long-Term Protection in ARPE-19 Cells through Its Effects on Nrf2 Activation and Phase 2 Gene Expression. *Investig. Ophthalmol. Vis. Sci.* **2009**, *50*, 2398. [CrossRef] [PubMed]
31. Lee, S.; Yang, H.; Son, G.; Park, H.; Park, C.-S.; Jin, Y.-H.; Park, Y. Eriodictyol Protects Endothelial Cells against Oxidative Stress-Induced Cell Death through Modulating ERK/Nrf2/ARE-Dependent Heme Oxygenase-1 Expression. *Int. J. Mol. Sci.* **2015**, *16*, 14526–14539. [CrossRef] [PubMed]
32. Liu, Y.; Wang, R.; Liu, H.; Tu, Z. Dietary Phytochemicals Targeting NRF2 against Skin Cellular Senescence: Mechanistic Insights and Potential for Functional Food Development. *Biology* **2025**, *15*, 39. [CrossRef] [PubMed]

Disclaimer/Publisher's Note: The statements, opinions and data contained in all publications are solely those of the individual author(s) and contributor(s) and not of MDPI and/or the editor(s). MDPI and/or the editor(s) disclaim responsibility for any injury to people or property resulting from any ideas, methods, instructions or products referred to in the content.